IEEE Access
Multidisciplinary | Rapid Review | Open Access Journal

Received June 21, 2021, accepted July 12, 2021, date of publication July 26, 2021, date of current version August 10, 2021.

Digital Object Identifier 10.1109/ACCESS.2021.3100144

Designing Efficient Phase-Gradient Metasurfaces for Near-Field Meta-Steering Systems

KHUSHBOO SINGH [1,2], (Member, IEEE), MUHAMMAD U. AFZAL [2], (Senior Member, IEEE), AND KARU P. ESSELLE [2], (Fellow, IEEE)

[1]School of Engineering, Macquarie University, Macquarie Park, NSW 2113, Australia
[2]School of Electrical and Data Engineering, University of Technology, Ultimo, NSW 2007, Australia

Corresponding author: Khushboo Singh (khushboo.singh@uts.edu.au)

This work was supported in part by the Australian government international Research Training Pathway (iRTP) scholarship and in part by the Australian Research Council (ARC) discovery grant and University of Technology Sydney (UTS), Faculty of Engineering and Technology (FIET) seed grant.

ABSTRACT We investigate the aptness of various 4^{th} order (90°) rotationally symmetric phase-transforming cells for the upper phase-gradient metasurface, which always receives an oblique incidence wave from the lower metasurface in a Near-Field Meta-Steering system. A comprehensive study on the behavior of various phase-transforming cells and corresponding supercells when a rotating oblique plane wave impinges on them is presented. First, we select the supercell with high transmission in the desired output Floquet modes, for both TE and TM input modes, when an oblique incidence wave is rotated. The selected supercell is then optimized using Floquet analysis in conjunction with particle swarm optimization (PSO). All the undesired modes are successfully suppressed below −32 dB in the optimized supercell, and the predicted broadside radiation pattern is free of spurious grating lobes. A Near-Field Meta-Steering system with an aperture diameter of $7.3\lambda_0$ (110mm @ 20 GHz) is presented. It has a pair of optimized phase-gradient metasurfaces and a dipole antenna array. A maximum peak directivity of 24.2 dB is achieved when the beam is in the broadside direction. The proposed steering system is capable of scanning a conical range with an apex angle of 126° when a 6 dB reduction in peak directivity is allowed. For a 3 dB variation in the peak directivity, the corresponding apex angle is 103°.

INDEX TERMS Near-field phase transformation, beam-steering, high-gain antenna, phase gradient metasurfaces, lens antenna, flat-panel, flat lens, transmitarray, reflectarray, Risley prism, metamaterial, satellite communication, 5G, SOTM, COTM, satellite TV, RLSA, EBG, SLL.

I. INTRODUCTION

Highly directive beam-steering antennas are indispensable components in satellite communication-on-the-move (SOTM) systems to establish seamless connectivity between ground receivers and satellites. The antennas with planar profiles and wide-angle beam-steering capabilities are of great interest to the industry because of their suitability in low-earth-orbit based satellite communications [1]–[3]. Far-field patterns, including sidelobes and grating lobes of the antennas for SOTM and future wireless systems, must conform to strict regulatory standards while the beam is being steered. Therefore, a robust approach is required in designing antenna systems to ensure high directivity and low SLLs with beam steering.

Several beam-steering techniques have been researched in the past to develop an efficient antenna system [4]–[6]. Among all, active electronically steerable arrays are attractive because of their thin and planar profile [7]–[11]. However, at high frequencies and for high-gain (> 30 dB) applications, these systems incur heavy power losses in the feed network as well as in RF components such as phase shifters and PIN diodes [12], [13]. Therefore, heat dissipation poses an additional design challenge in such systems. In contrast, a passive beam-steering system such as variable inclination continuous transverse stub antenna array does not need active elements or a lossy feed network [14], [15]. Because of this advantage, different passive-steering techniques have been investigated in the last decade. A *sliding aperture*

The associate editor coordinating the review of this manuscript and approving it for publication was Weiren Zhu.

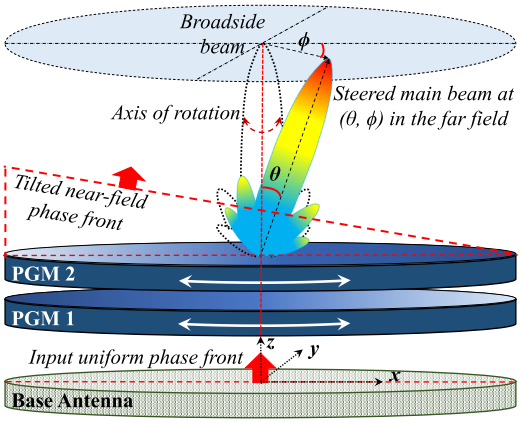

FIGURE 1. Configuration of a Near-Field Meta-Steering system.

based design in [16] uses the in-plane translation of thin metasurface lenses, placed at a few wavelengths above a feed, to steer the beam in the elevation. In [17]–[19], both in-plane feed translation (for elevation scanning) and antenna rotation (for azimuth scanning) are implemented for beam-steering. In [20]–[22], an improved passive beam-steering technique is presented, which uses a pair of phase-gradient metasurfaces (PGMs) placed at one or less than a wavelength spacing from the feeding base antenna. These metasurfaces are rotated synchronously and independently to steer the beam in a large conical region. A demonstration of this technique with a medium-aperture resonant-cavity antenna (RCA) shows beam steering in a cone of apex angle of 102° [20]. Owing to the use of near-field metasurfaces, this method is also referred to as Near-Field Meta-Steering (NFMS) [23]. The NFMS has several advantages, including low-power consumption, low cost, high power handling capability, polarization flexibility, and the ability to maintain planar geometry while the beam is steered.

Researchers across the world have reported several trail-blazing developments on NFMS [24]–[28] following the first paper published in 2017 [20]. One of the developments is the antenna system designed for high-power applications with cross-slots based all-metal metasurfaces [27] similar to an all-metal transmitarray [29]. An accurate method to analytically predict the beam location in spherical coordinates (Θ and Φ) was presented in [30]. A Floquet analysis-based approach to reduce the most offending grating lobes that appear during beam-steering in a Near-Field Meta-Steering system has been proposed in [23]. The concept has been recently implemented to design a broadband millimeter-wave beam-steering system by placing a pair of dielectric structures very close to the aperture of the horn antenna in [31].

The configuration of a classic Near-Field Meta-Steering (NFMS) system is shown in Fig. 1. It has an antenna with RF connection at the base, referred to as ''base antenna'' hereafter, and a pair of independently rotating PGMs with no physical connection with the base antenna. The adjacent cells in PGMs are dissimilar in the x-direction, as shown in Fig 2, which renders them locally aperiodic. However,

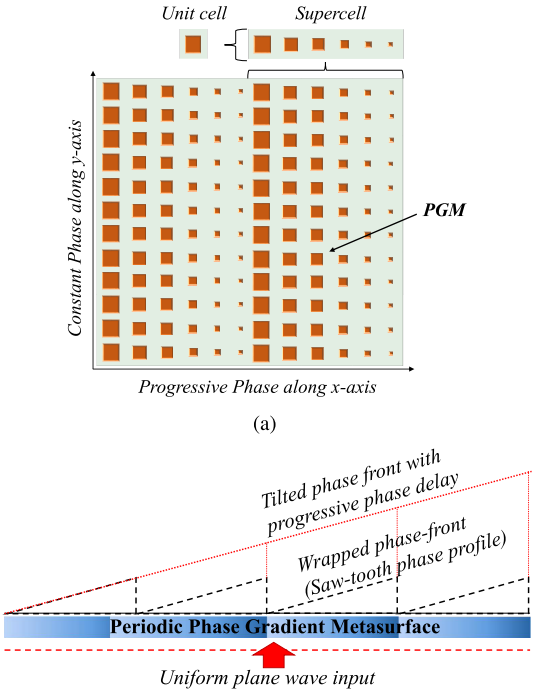

FIGURE 2. Configuration of a Phase-Gradient Metasurface. (a) A unit cell, a supercell and a phase-gradient metasurface. (b) Near field phase transformation introduced by phase-gradient metasurface.

a set of distinct cells (known as a supercell) is repeated periodically to create a full metasurface [23]. A supercell in a PGM is analogous to one period of a diffraction grating [32]. Therefore, a PGM essentially mimics the behavior of a blazed grating. Strong sidelobes and grating lobes constitute a significant concern in beam-steering antennas. The grating lobes are often more severe and hence problematic. Several endeavors to design refracting metasurfaces without spurious diffraction have been made in the past [33]–[35]. It has been observed that more grating lobes appear when the second PGM is placed above the first PGM and rotated to steer the beam in a NFMS system. Typically, the beam can be rotated within a 3D conical volume by only turning the upper PGM and keeping both the lower metasurface and the base antenna fixed. In this work, we primarily focus on steering systems where the upper PGM is the only moving component, while the base antenna and lower PGM are assumed fixed at all times. In all previous NFMS systems, the two metasurfaces were designed using normal incidence input. However, in practice, the second metasurface always receives an oblique incident wave. Furthermore, the polarization changes due to relative rotation between the first and second metasurface while steering the beam. This work presents a different approach to design the second (upper) metasurface by considering the oblique nature of the incident plane waves.

To design a beam-steering system with low SLLs for all steering angles, we investigate several phase-transforming cells (PTCs) and corresponding supercells for their response

to the rotation of an obliquely incident plane wave to judge their suitability for designing the upper PGM. At first, various PTCs with 4^{th} order (90°) rotational symmetry were explored, and their response to oblique incidence with changing azimuth angle ϕ_{in} was recorded. PTCs with stable transmission magnitude and phase response to rotating oblique incidence are necessary but not sufficient to ensure better upper PGM performance since the neighboring cells in a PGM are distinct. The mutual coupling varies with the rotation of the obliquely incident wave. Therefore, we continued the investigation at the supercell scale, which includes the effect of mutual coupling. Floquet-based power analysis was performed on several supercells, which were excited with oblique incidence oriented at angles θ_{in} (elevation) and ϕ_{in} (azimuth). The total power transmitted in the desired output Floquet modes (the sum of power in TE and TM output modes that correspond to the main beam in desired direction) for a given θ_{in} and varying ϕ_{in} from 0° to 360° was recorded. The supercell with the high overall transmission in the desired direction as a function of ϕ_{in} rotation for both TE and TM incidence is expected to work best for rotating upper PGM design. We also investigate the effect of PTC size on the performance of upper PGM by comparing the performance of two supercells designed using similar PTCs with different lateral dimensions. The supercell with higher overall transmission in the desired direction, for both TE and TM oblique incidence, when ϕ_{in} is varied a complete cycle, was selected for the upper PGM design. The lower PGM was designed using the conventional procedure explained in [20], [23]. A supercell-pair with the upper supercell placed a quarter wavelength above the lower supercell was optimized using the PSO algorithm inbuilt in CST MWS. A full PGM-pair was then designed using the optimized supercell-pair and is excited with an array of dipoles. The steering performance of the metasurface was studied and explored for several orientations. We provide a general framework to design efficient PGMs for the NFMS systems, based on the nature of incident wave and considering the variable relative rotation between the PGM pairs in the NFMS system while steering the beam. This investigation will help the engineers make an educated decision when designing a NFMS system.

The contents of this manuscript are organized as follows. Section II performs a detailed study on several PTCs with 4^{th} order (90°) rotational symmetry to predict their aptness for upper rotating PGM design. A Floquet based power analysis is presented for several supercells. The transmission response of supercells as a function of oblique incidence wave rotation is investigated. The best performing supercell is optimized using a Floquet based optimization approach in conjunction with the PSO algorithm in CST MWS. Section III describes a NFMS system designed using an array of dipoles as the base antenna and a pair of optimized PGMs. The steering performance for several beam locations is provided as Cartesian plots of elevation plane radiation pattern cuts and 2D contour plots of far-field patterns. Section IV provides conclusion.

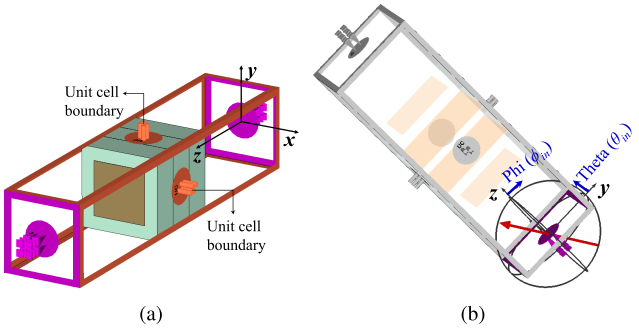

FIGURE 3. Simulation set-up for a PTC for the upper PGM in a NFMS system. (a) Perspective view of a square metal patch PTC with unit cell boundary conditions and (b) oblique incidence plane wave direction defined by θ_{in} and ϕ_{in}.

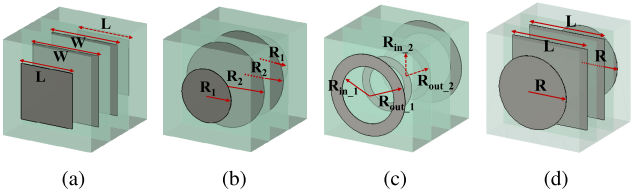

FIGURE 4. Phase transforming cells (a) Type-A (b) Type-B (c) Type-C (d) Type-D.

II. METHOD

A. ANALYSIS OF PTCs WITH 4^{th} ORDER ROTATIONAL SYMMETRY

PTCs with 4^{th} order (90°) rotational symmetry are used to design the PGMs for circularly polarized antenna systems because they have identical responses to both TE and TM-polarized waves that are incident normally. In this analysis, the PTCs are simulated with periodic boundary conditions, as shown in Fig. 3. The unit cell boundary conditions are applied along x- and y-directions as shown in Fig. 3(a). The PTC is excited with an obliquely incident TE or TM-polarized plane wave. The oblique-incident wave propagation vector shown by the red arrow in Fig. 3(b) is defined in terms of θ_{in} and ϕ_{in}, where θ_{in} is the oblique elevation angle, and ϕ_{in} is the azimuth angle. As mentioned above, the oblique incidence analysis is specifically carried out for the PTCs in the upper metasurface. Here, θ_{in} is equal to the beam tilt angle of the lower PGM, while ϕ_{in} represents the relative rotation between the upper and lower metasurfaces in the NFMS system. In this way, we can set up an environment in which the PTCs of upper PGM operate and investigate their performance accordingly.

All the PTCs considered in this investigation have three dielectric layers (1.575 mm thick Taconic TLY 5 with $\epsilon_r = 2.2$) sandwiched between four printed metal-patch layers and are designed to operate at 20 GHz. Here A, B, C, and D represent different types of PTCs, as shown in Fig. 4. Type-A has square metal patches in all four layers. Type-B has circular metal patches in all four layers. Type-C has circular ring-shaped metal patches in all four layers. Type-D has circular metal patches on the top and bottom layers and square metal patches on the second

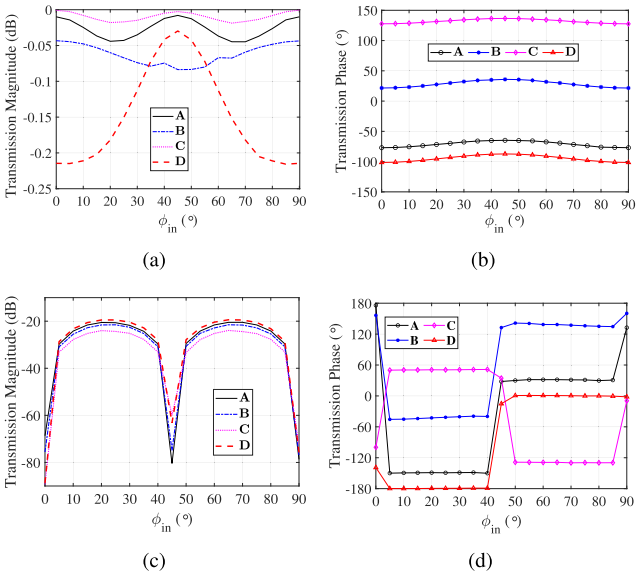

FIGURE 5. Transmission response of PTCs for oblique incidence. (a) Transmissions magnitudes of the TE output mode. (b) Transmissions phases of the TE output mode. (c) Transmissions magnitudes of the TM output mode. (d) Transmissions phases of the TM output mode.

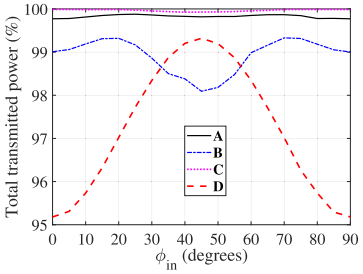

FIGURE 6. Total power transmitted (the sum of power in both TE and TM output modes) as a percentage of total incident power versus ϕ_{in}.

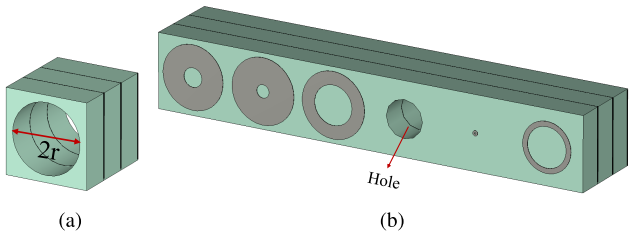

FIGURE 7. A supercell with a hole. (a) Type-E PTC with a hole. (b) A supercell designed using Type-C cells having ring-shaped metal patches and a Type-E cell (with a hole) for 26° beam-tilt.

and third layers. Each PTC has a side length of 4.3 mm (approximately $\lambda_0/3.5$ @ 20 GHz).

Fig. 5 shows the transmission magnitude and phase responses of all PTCs, A, B, C, and D, when they are illuminated by an obliquely incident TE-wave with an incident angle $\theta_{in} = 35°$. The wave direction angle ϕ_{in} is varied from 0° to 90° at a step of 5°. Due to 4^{th} order rotational symmetry, the transmission response for any other ϕ_{in} can be deduced from these results. The transmission magnitudes and phases of the TE-mode output are shown in Fig. 5(a) and 5(b), respectively. Fig. 5(c) and 5(d), respectively shows the transmission magnitudes and phases of the TM output mode. For an oblique incidence wave with constant elevation angle θ_{in}, the response of the PTCs varies with respect to the change in ϕ_{in}, due to the variation in mutual coupling between the patches of the neighboring cells. In Fig. 6, the total transmitted power in the desired direction (the sum of power in both TE and TM output modes) is plotted against ϕ_{in}. We observe that C shows least variation in transmitted power with ϕ_{in}, followed by A, B and D. It is evident that to avoid spurious diffraction and concentrate maximum energy in the desired direction, a PTC with ring-shaped, square, or circular patches is a better choice compared to the PTC with a combination of circular and square patches.

The PTCs with less rotation sensitivity and high transmitted power is desirable but not sufficient to guarantee better performance in the upper PGM of a NFMS system. In a PGM, the neighboring cells are not identical, and hence the mutual coupling between adjacent cells is not captured accurately when a PTC is simulated with periodic boundary conditions. A periodic supercell accurately models the mutual coupling between the neighboring cells in a PGM. Therefore, a similar investigation is done in the next section for the periodic supercells in the upper rotating PGM of a NFMS system.

B. SUPERCELL DESIGN APPROACH

Based on our experience with Floquet analysis in CST, it is more accurate to design supercells with phase wrapping in the middle to avoid potential errors due to a periodic boundary aligned with a phase wrapping point on the edges, as in the conventional supercell designs. For the upper PGM, the PTCs are simulated with an oblique incidence θ_{in} equal to the lower PGM beam tilt, and ϕ_{in} is set as zero. The transmission response of all the PTCs is recorded after sweeping the dimensions of metal patches from minimum to maximum and stored in Database-I. Note that the patches in cell types A, B, C, and D increase the phase shift.

Next, in order to reduce phase shift, a new cell Type-E is created as follows. Metal patches are removed from all four layers in PTC, and a hole is drilled, as shown in Fig 7(a). This new PTC is excited with the same oblique incidence as before, and a parameter sweep is run on the radius of the hole. The transmission response obtained from parameter sweep on the hole-radius of Type-E PTC is stored in Database-II. As expected, the transmission phase of this PTC is much less than the lowest transmission phase obtained from Type-A to Type-D PTCs with metal patches. Conventionally, a PTC with the smallest or no metal patch is selected to achieve the lowest phase shift. In this design approach, the Type-E PTC with a hole provides a much lower transmission phase. The hole size is cautiously selected such that the structure is not susceptible to break, and the PTC has a high transmission magnitude. The transmission phase of this PTC (Type-E) is set as the reference phase, and all the other transmission phases in Database-I are normalized relative to this reference.

TABLE 1. Dimension of metal patches in each supercell design in (mm).

Supercell-A (L_i , W_i)		Supercell-B ($R1_i$, $R2_i$)		Supercell-C (Rout_1_i , Rout_2_i, d)			Supercell-D (L_i , R_i)	
$L_1 = 3.4$	$W_1 = 3.5$	$R1_1 = 1.95$	$R2_1 = 1.95$	Rout_$1_1 = 1.9$	Rout_$2_1 = 1.95$	$d_1 = 0.2$	$L_1 = 3.6$	$R_1 = 1.8$
$L_2 = 3.3$	$W_2 = 3.8$	$R1_2 = 2$	$R2_2 = 2.05$	Rout_$1_2 = 1.75$	Rout_$2_2 = 1.8$	$d_2 = 0.7$	$L_2 = 3.7$	$R_2 = 1.9$
$L_3 = 3.5$	$W_3 = 3.8$	$R1_3 = 2$	$R2_3 = 2.1$	Rout_$1_3 = 1.73$	Rout_$2_3 = 1.65$	$d_3 = 0.9$	$L_3 = 2.05$	$R_3 = 3.7$
$h_r = 1.45$		$h_r = 1.54$		$h_r = 1.45$			$h_r = 1.8$	
$L_5 = 1.6$	$W_5 = 1.9$	$R1_5 = 0.8$	$R2_5 = 1.2$	Rout_$1_5 = 0.75$	Rout_$2_5 = 1$	$d_5 = 0.3$	$L_5 = 1.8$	$R_5 = 0.55$
$L_6 = 1.4$	$W_6 = 2.9$	$R1_6 = 0.55$	$R2_6 = 1.7$	Rout_$1_6 = 0.35$	Rout_$2_6 = 1.65$	$d_6 = 0.1$	$L_6 = 2.8$	$R_6 = 0.65$
$L_7 = 3$	$W_7 = 3$	$R1_7 = 1.7$	$R2_7 = 1.75$	Rout_$1_7 = 1.6$	Rout_$2_7 = 1.6$	$d_7 = 0.6$	$L_7 = 3$	$R_7 = 1.6$
$L_8 = 3.6$	$W_8 = 2.9$	$R1_8 = 2.05$	$R2_8 = 1.65$	Rout_$1_8 = 1.95$	Rout_$2_8 = 1.7$	$d_8 = 0.2$	$L_8 = 3.4$	$R_8 = 1.7$

The supercells are then designed by choosing appropriate PTCs with high transmission magnitude and desired normalized phase values. An example supercell designed for 26° beam-tilt is shown in Fig. 7(b). Ideally, a total phase shift range of 360° (2π radians) is required to design a supercell that is periodically repeated along x and y-direction to form a full PGM. The absolute value of the highest transmission phase (ϕ_{max} in degrees) required to design a supercell is determined by the lowest achievable transmission phase shift (ϕ_{min}) from the constituent PTCs such that $\phi_{max} = \phi_{min} + 360$. Thus, lower the value of ϕ_{min} lower will be the ϕ_{max} and vice-versa. The transmission phase shift of a PTC of a given dimension increases with the increase in the size of metal patches. For higher values of ϕ_{max} the patch will be larger, and so will the mutual coupling between the adjacent cells. Since the value of ϕ_{min} achieved from a PTC with a hole is relatively smaller, this supercell design approach intrinsically avoids the need for using large metal patches, which leads to the strongest undesired mutual coupling.

C. EFFECT OF METAL PATCH GEOMETRY

It is crucial to analyze the supercell performance of the upper PGM as a function of rotation. To this effect, we investigated several supercells for their response to a rotating obliquely incident wave. Each supercell is simulated with periodic (unit cell) boundary condition and is excited with plane wave obliquely incident with constant θ_{in} and varying ϕ_{in} originating from the input Floquet port at the bottom. Using a Floquet analysis based approach [23], the total power transmitted in the desired output modes (the sum of power in TE and TM output modes that correspond to the main beam in desired direction) is recorded against several values of ϕ_{in}. A higher variation in power transmitted into the desired direction with rotation (varying ϕ_{in}) indicates more substantial mutual coupling variation, and such supercells shall be deemed unsuitable for upper PGM design.

We aim to achieve an elevation beam tilt Θ_{max} of at least 60° from the NFMS systems. Thus, each PGM should at least provide 25.7° beam-tilt to achieve combined steering up to 60° according to:

$$\sin\Theta_{max} = \sin\delta_1 + \sin\delta_2 \tag{1}$$

where δ_1 and δ_2 are the individual beam tilts of lower and upper metasurfaces. Since the two PGMs used in our NFMS system are designed to provide the same beam tilt, $\delta_1 = \delta_2 = \delta$. The maximum beam tilt is obtained when both upper and lower PGMs are aligned. We chose to examine the PGMs for two tilt angles (δ), for instance, 26° (<30°) and 36° (>30°), both of which can fulfill the beam-scanning range requirement of 60°.

Four different supercells, namely Supercell-A, Supercell-B, Supercell-C, and Supercell-D, were designed using corresponding PTC types A, B, C, and D, respectively, using the approach described earlier (Fig. 7(b)). Each PTC has a lateral dimension of $\lambda_0/3.8$. Each of these supercells were simulated with unit cell (periodic) boundary conditions in the frequency domain solver of CST MWS. An oblique linearly polarized plane wave (fundamental Floquet mode TE(00) or TM(00)) impinges on the supercell from the input Floquet port at the bottom. The power transmitted to each output Floquet mode was recorded, and the total percentage power in the desired direction was calculated. This process is repeated for different values of ϕ_{in} in the oblique incidence. The supercell response was investigated for both TE and TM incidence.

1) SYSTEM-I (PGMs WITH $\delta = 26°$)

Each PGM in this NFMS system has a beam tilt angle of 26°. Each of the four supercells were designed using one Type-E cell with hole and seven cells of the same type (A, B, C or D) with desired transmission phase and high transmission magnitude (≥ -1dB). The cells are arranged such that the progressive phase delay between adjacent cells is 45°. The geometrical parameters for each supercell are provided in Table 1. The index "i" denotes the cell number in the supercell. There are 8 unique PTCs in each supercell; thus $i = 1, 2, 3 \ldots 8$. The variable "d" is a unit-less parameter that represents the inner radius divided by outer ring radius in Supercell-C and it varies between 0.1 to 0.9.

When an oblique plane wave with $\theta_{in} = 26°$ and $\phi_{in} = 180°$ is incident at the input Floquet port, we obtain a nearly uniform phase distribution at the output of the supercell. This phase distribution in the near field produces a broadside radiation pattern in the far field. Variation in ϕ_{in} (which is equivalent to the rotation of the upper PGM in a NFMS system) steers the main beam in the radiation pattern, and the beam direction (Θ, Φ) can be calculated using the mathematical expressions derived from the phase

TABLE 2. Total power transmitted to the desired output modes (the sum of power in TE and TM output modes that correspond to the main beam in desired direction) in System-I for changing ϕ_{in}.

Supercell		Supercell-A		Supercell-B		Supercell-C		Supercell-D	
Input Mode		TE(00)	TM(00)	TE(00)	TM(00)	TE(00)	TM(00)	TE(00)	TM(00)
ϕ_{in}	Θ	Power (%)	Power (%)	Power (%)	Power (%)	Power (%)	Power (%)	Power (%)	Power (%)
180°	0°	86.7	79.6	84.9	73.4	67	75.6	82.1	71.4
135°	19.6°	77.2	81.5	73.7	75.3	68	73.3	75	78.7
90°	38.3°	73.1	78.8	65.8	78.9	62.3	69.1	67.1	80.8
45°	46.1°	64.7	75.2	59.5	74	53.1	69.6	48.4	70.5
0°	61.2°	57.8	59.5	66.2	45.4	53.6	54.6	59.4	54.3

TABLE 3. Direction of the main beam of System-I for different directions of the incident wave.

Oblique Incidence Parameters		Beam Direction	
θ_{in}	ϕ_{in}	Θ	Φ
26°	180°	0°	90°
26°	135°	19.6°	67.5°
26°	90°	38.3°	45°
26°	45°	46.1°	22.5°
26°	0°	61.2°	0°

method [30]:

$$\Theta = \sin^{-1}\left\{\frac{1}{k_0}\sqrt{p_1^2 + p_2^2 + 2p_1p_2\cos(\psi_1 - \psi_2)}\right\} \quad (2)$$

$$\Phi = \tan^{-1}\left\{\frac{p_1\sin\psi_1 + p_2\sin\psi_2}{p_1\cos\psi_1 + p_2\cos\psi_2}\right\}, \quad (3)$$

$$\text{where } p_i = k_0\sin\delta_i, (i = 1, 2) \quad (4)$$

and Θ, Φ, δ_1, δ_2, ψ_1 and ψ_2 are the elevation angle of the main beam in the radiation pattern, the azimuth angle of the main beam in the radiation pattern, beam tilt angle for lower PGM, beam tilt angle for upper PGM, the orientation angle of lower PGM and orientation angle of upper PGM, respectively. For $\delta_1 = \delta_2 = \delta$:

$$\Theta = \sin^{-1}\left\{\sin(\delta)\sqrt{2(1 + \cos(\psi_1 - \psi_2))}\right\} \quad (5)$$

$$\Phi = \frac{\psi_1 + \psi_2}{2} \quad (6)$$

Using (5) and (6), the beam direction corresponding to five incident plane wave directions are calculated and listed in Table 3. A maximum beam tilt of 61.2° is achieved for $\theta_{in} = 26°$ and $\phi_{in} = 0°$, that represents the PGM orientation in which the two PGMs are aligned (i.e. $\psi_1 = \psi_2 = 0°$). Note that $\phi_{in} = \psi_2 - \psi_1$. In case of our NFMS system, the upper and lower metasurfaces have same phase gradients, thus, $\delta_1 = \delta_1 = \delta = 26°$. Hence, for this orientation $\Theta = \sin^{-1}\{2\sin(\delta) = 61.2°\}$ from (5) and $\Phi = 0°$ from (6). The variation in ϕ_{in} corresponds to the variation in the orientation angle of upper PGM, ψ_2, relative to the fixed lower PGM ($\psi_1 = 0°$). The transmission characteristics of each supercell were investigated for both TE and TM incidence.

The total percentage output power in the desired direction for different values of ϕ_{in} are provided in Table 2. It is evident from Table 2 that supercell-A has better overall performance than the other three supercells. For both TE and TM incidence, transmitted power in the desired direction does not fall below 50% for any orientation. Supercell-C also exhibits a relatively lesser variation in transmitted output power with changing ϕ_{in} but suffers from high spurious diffraction. The incident power deflects to other undesired Floquet modes, which results in lower power transmission to the desired direction. For Supercell-B, the performance deteriorates for TM incidence and the total power in the desired direction drops to less than 50% for extreme beam-tilt (61.2°). In Supercell-D, the transmitted power falls below 50% for a 46° beam tilt.

2) SYSTEM-II (PGMs WITH $\delta = 35.5°$)

Each PGM in this NFMS system has a beam tilt angle of 35.5°. A new set of four supercells were designed as before using PTCs with the desired transmission phases and high transmission magnitudes ($\geq -1dB$). When an oblique plane wave with $\theta_{in} = 35.5°$ and $\phi_{in} = 180°$ is incident from the input Floquet port, we obtain a uniform phase distribution at the output of the supercell and hence the main beam in the broadside direction (i.e. $\Theta = 0°$). Unlike in System-I, in this system the main beam moves to "invisible" region for smaller value of ϕ_{in} from 0° to 61°, due to large phase gradients of PGMs. The main beam stays in the visible upper hemisphere for the range of ϕ_{in} from 61° to 180°. The value of ϕ_{in} was decreased from 180° to 82°, which steers the beam from 0° to 61.2°. Table 6 shows the main-beam direction in the far-field pattern for different oblique incidence orientations.

The geometrical parameters for each supercell are provided in Table 4. The cells are arranged such that the progressive phase delay between adjacent cells is 60°. The index "i" denotes the cell number in the supercell. There are 6 unique PTCs in each supercell; thus $i = 1, 2, 3 \ldots 6$. The variable "d" is a unit-less parameter that controls the inner radius of the ring in Supercell-C, and it varies between 0.1 to 0.9. The total power transmitted to the desired output Floquet modes (corresponding to main beam) for several orientations of oblique incidence is shown in Table 5. It is observed from Table 5 that Supercell-B performs better for both TE and TM incidence. For Supercell-C and Supercell-D, the power transmitted in the desired direction falls below 50% for 61° beam tilt. Supercell-A also performs reasonably well for both TE and TM incidence, but Supercell-B outperforms supercell-A for both cases. It is vivid that supercells with

TABLE 4. Dimension of metal patches in each supercell design in (mm).

Supercell-A (L_i , W_i)		Supercell-B ($R1_i$, $R2_i$)		Supercell-C ($Rout\_1_i$, $Rout\_2_i$, d)			Supercell-D (L_i , R_i)	
$L_1 = 3.3$	$W_1 = 3.3$	$R1_1 = 1.56$	$R2_1 = 1.91$	$Rout\_1_1 = 1.85$	$Rout\_2_1 = 1.9$	$d_1 = 0.3$	$L_1 = 3.4$	$R_1 = 1.7$
$L_2 = 3.3$	$W_2 = 3.7$	$R1_2 = 1.97$	$R2_2 = 2.06$	$Rout\_1_2 = 1.9$	$Rout\_2_2 = 2.05$	$d_2 = 0.2$	$L_2 = 3.7$	$R_2 = 1.8$
$L_3 = 3.5$	$W_3 = 3.8$	$R1_3 = 1.9$	$R2_3 = 2.1$	$Rout\_1_3 = 1.9$	$Rout\_2_3 = 1.9$	$d_3 = 0.6$	$L_3 = 3.7$	$R_3 = 2$
$h_r = 1.25$		$h_r = 1.62$			$h_r = 1.1$		$h_r = 1.8$	
$L_5 = 1.1$	$W_5 = 2.6$	$R1_5 = 0.83$	$R2_5 = 1.3$	$Rout\_1_5 = 0.15$	$Rout\_2_5 = 1.55$	$d_5 = 0.3$	$L_5 = 2.2$	$R_5 = 0.8$
$L_6 = 2.8$	$W_6 = 2.9$	$R1_6 = 1.28$	$R2_6 = 0.83$	$Rout\_1_6 = 1.45$	$Rout\_2_6 = 1.55$	$d_6 = 0.8$	$L_6 = 2.9$	$R_6 = 1.45$

TABLE 5. Total power transmitted to the desired output modes (the sum of power in TE and TM output modes that correspond to the main beam in desired direction) in System-II for changing ϕ_{in}.

Supercell		Supercell-A		Supercell-B		Supercell-C		Supercell-D	
Input Mode		TE(00)	TM(00)	TE(00)	TM(00)	TE(00)	TM(00)	TE(00)	TM(00)
ϕ_{in}	Θ	Power (%)	Power (%)	Power (%)	Power (%)	Power (%)	Power (%)	Power (%)	Power (%)
180°	0°	93.6	77.3	94.5	83.9	94.1	76.8	85.6	75.4
146°	19.85°	76.4	70.2	76.4	79.4	89.1	75.2	63.8	77.8
115°	38.6°	78.1	77.9	87.9	89.8	80.3	75.1	71.9	75.6
103°	46.3°	75.6	79	72.3	73.3	74.5	58.1	66.2	70
82°	61.2°	51.3	55	62.9	61.1	48.7	36.1	48.5	49.9

TABLE 6. Direction of the main beam of System-II for different directions of the incident wave.

Oblique Incidence Orientation		Steered Beam Location	
θ_{in}	ϕ_{in}	Θ	Φ
35.5°	180°	0°	90°
35.5°	146°	19.85°	73°
35.5°	115°	38.6°	57.5°
35.5°	103°	46.3°	51.5°
35.5°	82°	61.2°	41°

only square metal patches and supercells with only circular metal patches are judicious choices to design upper PGMs in a NFMS antenna system when combined with a Type-E cell with a hole. They exhibit less diffraction with rotation.

We now compare Supercell-A in System-I (hereafter referred to as System-IA) with supercell-B in System-II (hereafter referred to as System-IIB). The total power transmitted to the desired direction (main-beam) is plotted against the beam tilt (elevation angle Θ) in Fig. 8. It is observed that both System-IA and System-IIB perform well for both TE and TM incidence. System-IA shows a gradual variation in total transmitted power to the main beam with increasing beam tilt. On the other hand, System-IIB shows a non-monotonic response with comparatively higher transmitted power for broadside beam as well as around 38° and 60° beam tilts. For some other tilt angles, such as around 19° and 46°, transmitted power is slightly lower than System-IA. This study, indicates that System-IIB has a better overall performance over System-IA, mainly because the total power transmitted in the desired direction is relatively higher for most steering angles. One can also argue otherwise, but the fact that System-IIB performs well in both TE and TM incidence modes outweighs the choice of System-IA.

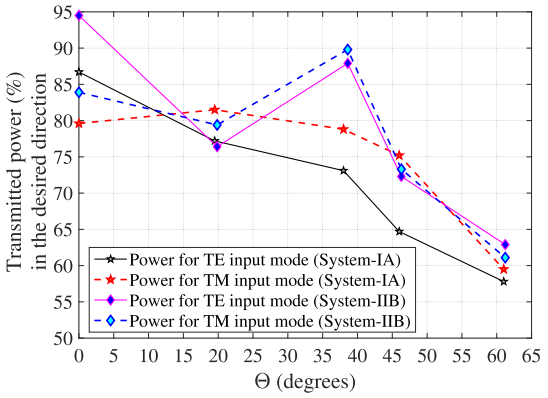

FIGURE 8. Variation of the total power transmitted in the desired direction (main beam) with the changing elevation steering angle Θ in System-IA and System-IIB.

D. EFFECT OF CELL SIZE

To establish an understanding of how the cell size affects PGM performance, we designed another set of PGMs with PTCs that are larger, around $\lambda_0/2.72$ long (approximately 5.5 mm @ 20 GHz). We chose to examine the PGMs for two tilt angles (δ), for instance, 27° ($< 30°$) and 33° ($> 30°$), both of which can fulfill the beam-scanning range requirement of $\Theta_{max} \geq 60°$. In the previous analysis, System-IA and System-IIB were found to perform reasonably well under variable ϕ_{in}. We now consider two new systems, namely System-III and System-IV. A set of two supercells was designed for each of these systems using relatively larger cell types A and B (approximately $\lambda_0/2.72$ long) along with one Type-E PTC with hole. The supercells were simulated with unit cell (periodic) boundary conditions in the frequency domain solver of CST MWS. The total power transmitted in the desired direction for different values of ϕ_{in} was calculated for both oblique TE and oblique TM incidence.

TABLE 7. Total power transmitted to the desired output modes (the sum of power in TE and TM output modes that correspond to the main beam in desired direction) in System-III for changing ϕ_{in}.

Supercell		Supercell-A		Supercell-B	
Input Modes		TE(00)	TM(00)	TE(00)	TM(00)
ϕ_{in}	Θ	Power(%)	Power(%)	Power(%)	Power(%)
180°	0°	82.9	81.7	84.1	80.1
136°	19.8°	80.2	83.7	80.7	83.4
93°	38.6°	79.9	79.5	78.2	80.3
75°	46.1°	71.8	81.2	72.3	84.0
30°	61.2°	66.6	72.2	69.6	79.1

TABLE 8. Total power transmitted to the desired output modes (the sum of power in TE and TM output modes that correspond to the main beam in desired direction) in System-IV for changing ϕ_{in}.

Supercell		Supercell-A		Supercell-B	
Input Modes		TE(00)	TM(00)	TE(00)	TM(00)
ϕ_{in}	Θ	Power(%)	Power(%)	Power(%)	Power(%)
180°	0°	92.8	79.8	95.1	78.9
144°	19.6°	86.4	86.7	92.5	85.4
110°	38.6°	81.1	77.8	88.5	91.3
97°	46.2°	76.9	78.9	81.4	88.6
73°	61.1°	60.9	79.6	72.9	90.6

1) SYSTEM-III (PGM WITH $\delta = 27°$)

Each PGM in this NFMS system has a beam tilt angle of 27°. Each of the two supercells were designed using one PTC of Type-E (a $\lambda_0/2.72$ PTC with hole) and 5 other cells of same type (A or B, of size $\lambda_0/2.72$) with desired transmission phases and high transmission magnitudes (≥ -1 dB). They are arranged such that the phase shift between adjacent PTCs is 60°. When an oblique plane wave with $\theta_{in} = 27°$ and $\phi_{in} = 180°$ is incident from the input Floquet port, a nearly uniform phase distribution is achieved at the output of the supercell. The beam is steered by changing the value of ϕ_{in}. Total power transmitted in the desired direction for different values of ϕ_{in} is shown in Table 7. We observe that both Supercell-A (System-IIIA) and Supercell-B (System-IIIB) perform well with changing ϕ_{in}, for TE as well as TM incidence. However, based on the fact that absolute power transmitted in the main-beam direction for maximum beam tilt is more for System-IIIB compared to System-IIIA, we consider System-IIIB to be better.

2) SYSTEM-IV (PGMs WITH $\delta = 33°$)

Each PGM in this NFMS system has a beam tilt angle of 33°. Each of the two supercells were designed using one Type-E PTC (a $\lambda_0/2.72$ PTC with hole) and 4 other PTCs of same type (A or B, of size $\lambda_0/2.72$) with desired transmission phases and high transmission magnitudes (≥ -1 dB). They are arranged such that the phase shift between adjacent PTCs is 72°. When an oblique plane wave with $\theta_{in} = 33°$ and $\phi_{in} = 180°$ is incident from the input Floquet port, a nearly uniform phase distribution is achieved at the output of the supercell producing a broadside radiation main beam. Unlike System-III where the main beam stays in the visible region for the entire range of ϕ_{in} from 0° to 180°, in this system, the main beam moves to "invisible" region for lower values of ϕ_{in} ranging from 0° to 46°. Total power transmitted in the main-beam direction for different values of ϕ_{in} are provided in Table 8. It is observed that Supercell-B (System-IVB) outperforms Supercell-A (System-IVA) for most beam locations. This shows that System-IVB is a better choice when designing a pair of rotating PGMs for a NFMS system. Also, both System-IVA and System-IVB perform better than System-IIIA and System-IIIB, which indicates that (for a given beam tilt) PGMs with steeper gradient are better. An overall observation on the performance of all four systems

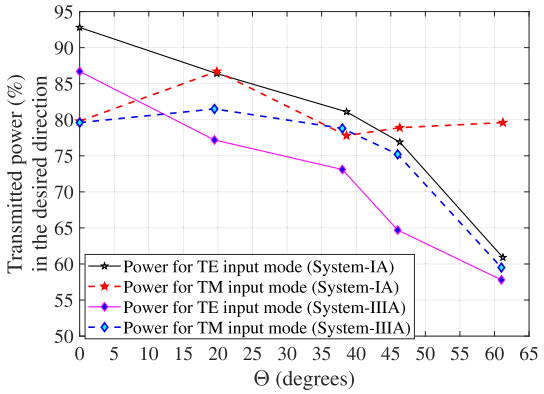

FIGURE 9. Variation of the total power transmitted in the desired direction (main beam) with the changing elevation beam-steering angle Θ in System-IA and System-IIIA.

shows that for a given maximum beam tilt angle, the bigger PTCs and corresponding supercells are a better choice to design PGMs for NFMS systems. To validate this claim we show a comparison between System-IA with System-IIIA in Fig. 9 and System-IIB with System-IVB in Fig. 10. The total power transmitted to the desired direction (main-beam) is plotted against the beam tilt (elevation angle Θ). From both these comparisons, we observe that the bigger supercells have a better transmission in the desired direction for both TE and TM incidence. Such a response can be justified because the distance between adjacent metal patches in a supercell composed of bigger PTCs is more than the ones designed using smaller PTCs. Hence, the effect of variation in mutual coupling with rotation is less.

E. OPTIMIZATION OF SUPERCELL-PAIR

System-IVB is the best among all the systems considered in the analysis carried out in this study. A pair of System-IVB supercells were then optimized to suppress the undesired grating lobes in an NFMS system.

For any optimization algorithm to provide the global best solution, the problem should be defined accurately. In a NFMS system, the PGMs always exist in pairs. To accurately model the optimization of such beam-steering systems, it is desirable to optimize both PGMs either separately or as a pair. Based on our experience, we can say that both approaches work well. However, the PGMs in our NFMS system always exist in pairs placed above the base antenna. Hence, to model

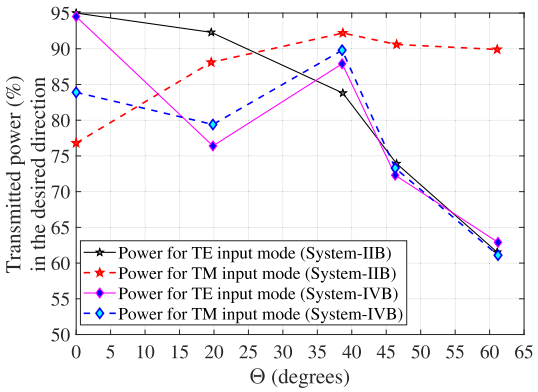

FIGURE 10. Variation of the total power transmitted in the desired direction (main beam) with the changing elevation beam-steering angle Θ in System-IIB and System-IVB.

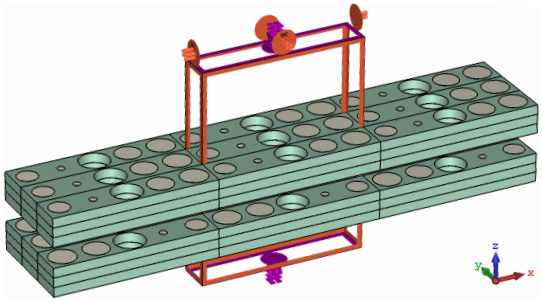

FIGURE 11. Full wave simulation setup for optimization of PGM-pair.

TABLE 9. Magnitude of transmitting and reflecting modes before and after optimization.

Modes	Magnitude (dB) Before Optimization	Magnitude (dB) After Optimization
T_0	-0.75	-0.26
T_{-1}	-22.40	-32.55
T_1	-26.07	-36.71
T_{-2}	-28.17	-35.01
T_2	-33.81	-46.67
R_0	-17.36	-33.38
R_{-1}	-9.54	-15.37
R_1	-17.10	-33.88
R_{-2}	-22.92	-25.24
R_2	-27.70	-27.75

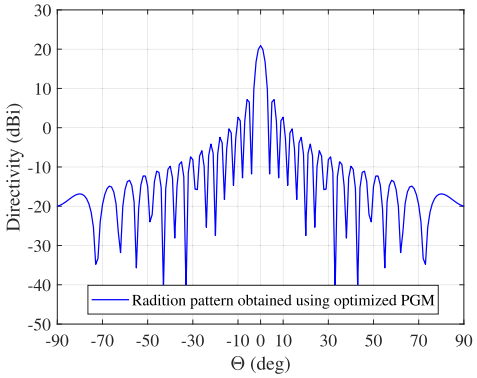

FIGURE 12. Broadside radiation pattern for a supercell-pair ($\psi_1 = 0°$ and $\psi_2 = 180°$) predicted using CST array calculator.

the real-time system more accurately, we optimized the pair of PGMs together. Besides, optimizing each PGM separately is time-consuming and needs more resources in terms of system memory and CST licenses.

A pair of System-IVB supercells are arranged one above the other as shown in Fig. 11. A Floquet based optimization similar to the one described in [23] have been implemented. The top supercell is placed quarter wavelength above the bottom supercell and is aligned opposite such that $\psi_1 = 0°, \psi_2 = 180°$. It should be noted that the distance between two PGM pair can be reduced to as low as $0.125\lambda_0$ without significantly affecting the performance of the steering system. To simulate the response of full PGM-pair, the EM simulator (CST MWS) implements periodic (unit cell) boundaries along both x and y-directions. It is excited with a uniform plane wave incoming from the input Floquet port. The expected beam location is in the broadside direction since the supercell simulation setup mimics the NFMS system when the PGM-pair is oriented such that $\psi_1 - \psi_2 = 180°$ [20].

The supercell-pair supports 10 propagating modes (5 transmitting and 5 reflecting). Optimization aims to increase the magnitude of the desired mode (which corresponds to the main beam) and suppress the undesired modes (which correspond to the spurious grating lobes). Here, mode T_0 is the desired transmitting mode while T_{-1}, T_1, T_{-2} and T_2 are the undesired transmitting modes. The goal FF is defined in (7) as a weighted sum of the above-mentioned objectives.

$$FF = [w_m\{\max(0, (-0.1 - DM))\}]^2 + \sum_{i=1}^{9}[w_i\{\max(0, (UDM - (-35)))\}]^2, \quad (7)$$

where w_m is the weight associated with the desired mode (DM), and w_i are the weights associated with the undesired modes (UDM). The value of w_m is fixed to 20, and w_i is varied between 1 to 19 depending on their magnitude in the far-field pattern. We also include the reflecting modes in the goal but deliberately provide them lesser weights than undesired transmitting modes. We mostly focus on suppressing the undesired transmitting modes and simultaneously maintaining a healthy balance among the reflecting modes to avoid excessive reflections from the surfaces.

The magnitudes of transmitting modes before and after optimization are listed in Table 9. All the undesired transmitting modes are below −32 dB. The desired transmitting mode T_0 is −0.26 dB. All reflections are maintained below −15 dB. The far-field pattern generated for optimized surface-pair using CST array calculator for 8 repetitions along x-direction and 40 repetitions along y-direction is shown in Fig. 12. The pattern is free of grating lobes since all the undesired modes are below −32 dB. This supercell combination is then used

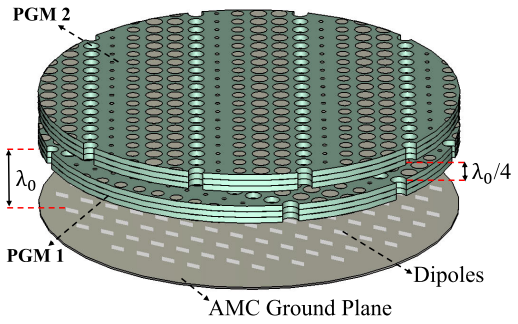

FIGURE 13. Near-Field Meta-Steering system designed using antenna array and a pair of PGMs.

to design a NFMS system with an array of dipoles as the base antenna.

III. IMPLEMENTATION

To design a Near-Field Meta-Steering system we need a base antenna preferably with uniform near-field phase distribution and a pair of PGMs. An array of dipoles with a half-wavelength inter-dipole spacing backed by an AMC ground plane placed very close below the array was used as the base antenna. The antenna array has a circular aperture of diameter $7.3\lambda_0$ (equal to 110mm @ 20GHz) with a total of 148 dipoles, and it provides a uniform plane wave output. Each array element was excited with Taylor-tapered amplitude distribution. The amplitude weights for all 148 array elements are generated in MATLAB using ''taylortaper'' and ''getTaper'' functions for a side-lobe level of -40 dB. The array pattern generated in CST has a directivity of 24.9 dBi, and the SLL is -38.9 dB. The supercell-pair optimized in the previous sections is used to generate a PGM-pair with an aperture of diameter $7.3\lambda_0$. The PGM-pair is a quarter wavelength apart and is placed a wavelength (λ_0) above the base antenna array. This assembly forms a Near-Field Meta-Steering system, shown in Fig. 13. The complete design process for NFMS system is provided as a flowchart in Fig. 14.

IV. RESULTS

The broadside radiation pattern after the addition of PGM-pair is shown in Fig 15. The directivity decreases from 24.9 dBi to 24.2 dBi, and the side-lobe level increases slightly by 0.8 dB compared to the pattern of the dipole antenna array without the metasurfaces. Typically, steer the beam in both elevation and azimuth planes, the PGMs are rotated. The complete mechanism of 2D beam steering using co-rotation and counter-rotation of PGM pair is elaborately discussed in [20]. In this work, only the upper PGM is rotated while the antenna and the lower PGM remain fixed to steer the beam in a 3D conical region. To get a clear picture of the beam pattern in a 3D space, we plot the 2D contour plot for the radiation pattern for a few beam positions in Fig 16. The 2D contour plots starting with the broadside beam until the beam is tilted to an elevation angle up to 60° is provided. All the significant minor lobes above −20 dB of the peak are shown

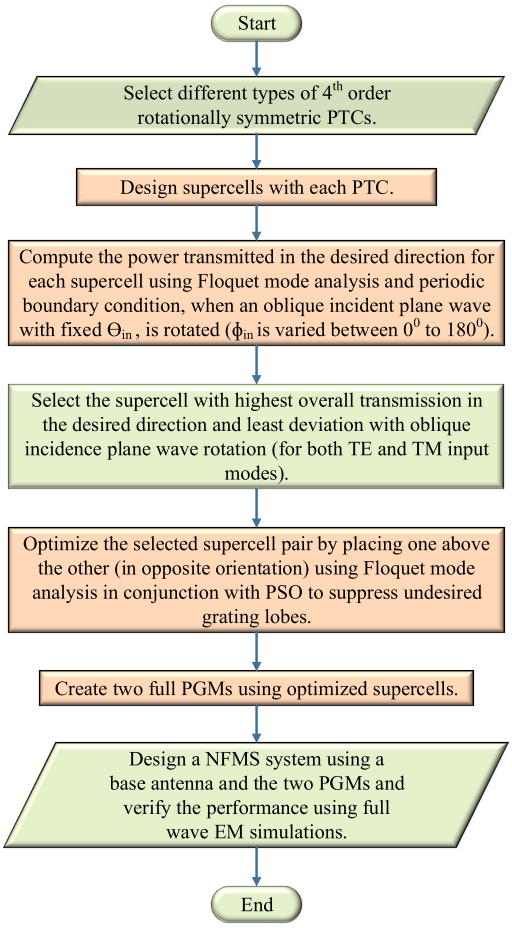

FIGURE 14. Steps to design an efficient Near-Field Meta-Steering system.

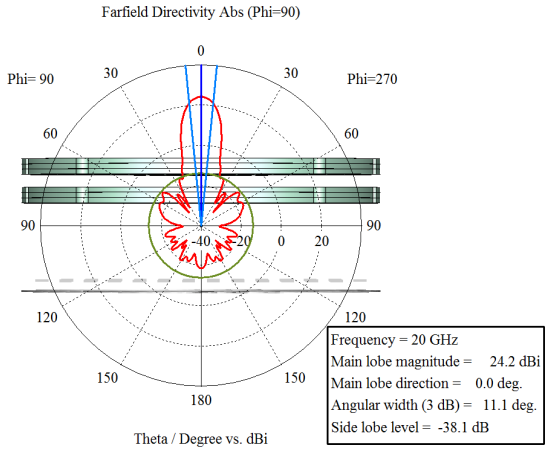

FIGURE 15. Near-Field Meta-Steering system with broadside radiation pattern.

in the plots. The proposed steering system can cover a conical region with an apex angle of 126° (63 × 2) with 6 dB reduction in directivity. The number of unwanted lobes increases with the increasing beam tilt.

The elevation pattern cut for several orientations of upper PGM is shown in Fig 17. The highest realized directivity is 24.2 dBi when the beam is in the broadside direction

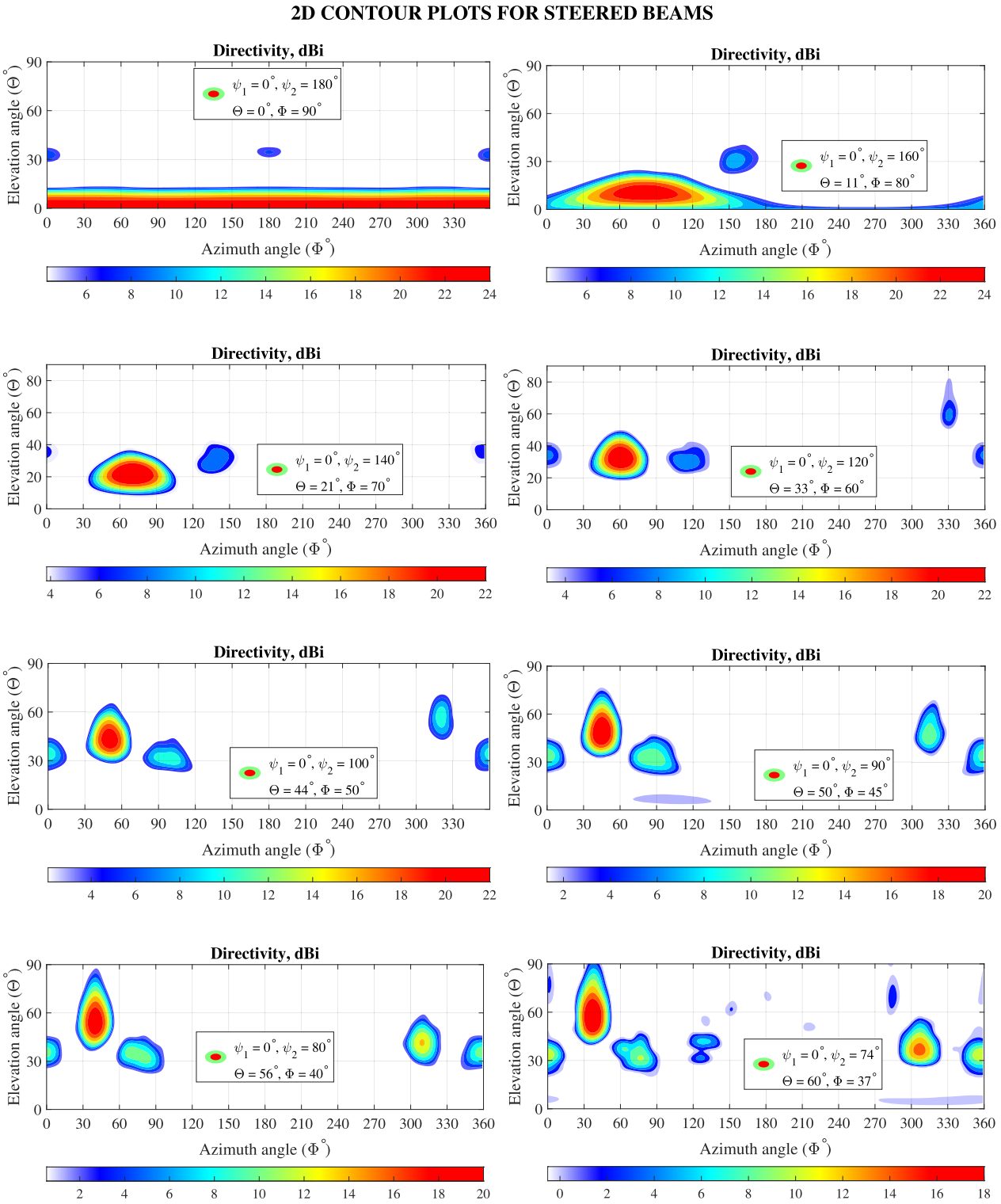

FIGURE 16. 2D far-field patterns for several beam orientations in a Near-Field Meta-steering system showing all grating lobes above −20 dB. The far-field pattern is steered from broadside $\Theta = 0°$ to $\Theta = 61°$ by rotating the upper PGM (varying ψ_2 from 180° to 74°).

($\Theta = 0°$). The peak directivity drops, and the beam gradually gets broader as the beam's elevation angle (Θ) increases. For a 3 dB reduction in the peak directivity, a maximum beam tilt of $\Theta = 50°$ is achieved. For a 6 dB reduction in the peak directivity, the beam can be steered to as large as 63° elevation tilt. The side-lobe level for all elevation pattern cuts is at least below −18 dB.

To visualize the beam-scan range in 2D angular space (Θ, Φ), we plot the -3 dB contours of the radiation patters as shown in Fig. 18. It is observed that all the elevation

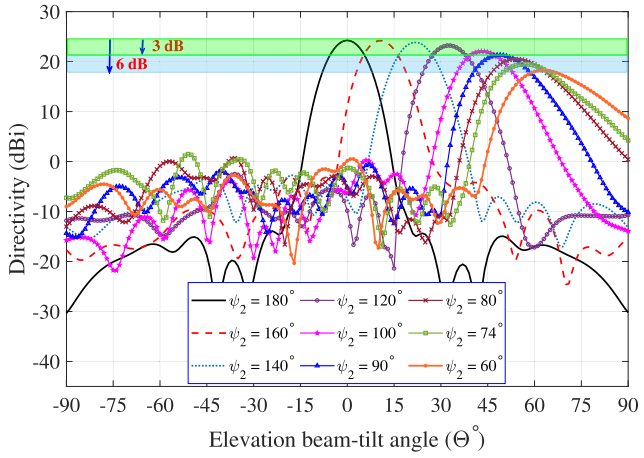

FIGURE 17. Elevation plane radiation pattern cuts for each rotation of PGM2 ($\psi_1 = 0$ at all times and only ψ_2 is varied).

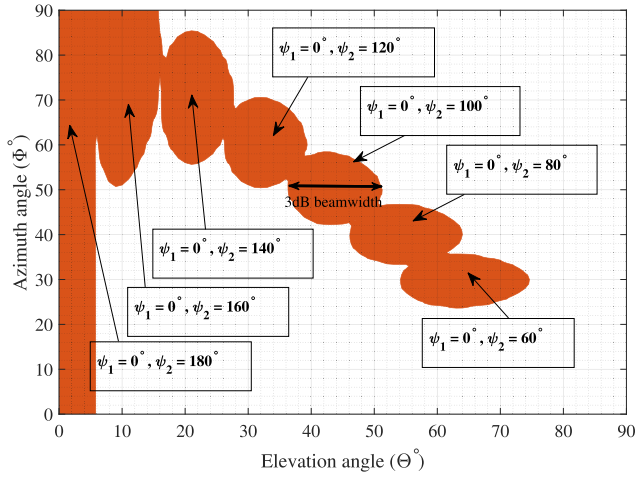

FIGURE 18. Contours of beam-scan coverage for several orientations of PGM2 when PGM1 is stationary.

angles ranging from 0° to 74° are covered. We do not plot the contours for elevation angles greater than 74° because the directivity dropped below -8 dB beyond this tilt angle. The results confirm that the proposed simple, low-profile, planar steering system can scan the beam in a conical volume with the apex angle of 148° (74 × 2).

V. CONCLUSION

A Floquet based power analysis of several supercells reveals that PGMs with circular metal patches have better performance when rotating, compared to other geometries with 4^{th} order rotational symmetry, like square, ring or a combination of square and circular metal patches. An investigation of the effect of supercell size on PGM performance, based on similar analysis shows that PGMs with bigger supercells or PTCs have better power transmission in the main-beam direction when rotating. The optimization of the best supercell selected based on the above-mentioned analysis suppressed all the undesired grating lobes below −32 dB, and the predicted far-field pattern is free of undesired grating lobes. The Near-Field Meta-Steering system designed using optimized PGMs can achieve a 3D beam coverage in a large conical volume.

REFERENCES

[1] O. Kodheli, E. Lagunas, N. Maturo, S. K. Sharma, B. Shankar, J. F. M. Montoya, J. C. M. Duncan, D. Spano, S. Chatzinotas, S. Kisseleff, J. Querol, L. Lei, T. X. Vu, and G. Goussetis, "Satellite communications in the new space era: A survey and future challenges," 2020, *arXiv:2002.08811*. [Online]. Available: http://arxiv.org/abs/2002.08811

[2] K. P. Esselle, "A brief overview of antenna technologies for communications-on-the-move satellite communication mobile terminals," in *Proc. IEEE Int. Symp. Antennas Propag. (APS)*, Jul. 2020, pp. 1637–1638.

[3] K. P. Esselle, "A brief overview of antenna technologies for communications-on- the-move satellite communication mobile terminals," in *Proc. IEEE Int. Symp. Antennas Propag. North Amer. Radio Sci. Meeting*, 2020, pp. 1637–1638, doi: 10.1109/IEEECONF35879.2020.9330396.

[4] I. Uchendu and J. R. Kelly, "Survey of beam steering techniques available for millimeter wave applications," *Prog. Electromagn. Res. B*, vol. 68, pp. 35–54, 2016.

[5] N. Gagnon and A. Petosa, "Using rotatable planar phase shifting surfaces to steer a high-gain beam," *IEEE Trans. Antennas Propag.*, vol. 61, no. 6, pp. 3086–3092, Jun. 2013.

[6] H. D. Griffiths and M. R. Khan, "Antenna beam steering technique using dielectric wedges," *IEE Proc. H, Microw., Antennas Propag.*, vol. 136, no. 2, pp. 126–131, Apr. 1989.

[7] Kymeta. (Mar. 10, 2014). *Kymeta Corporation to Demonstrate Its Metamaterials-Based Antenna at Satellite 2014*. Accessed: Jan. 31, 2021. [Online]. Available: https://www.kymetacorp.com/products/terminal/

[8] M. Boyarsky, T. Sleasman, M. F. Imani, J. N. Gollub, and D. R. Smith, "Electronically steered Nyquist metasurface antenna," 2020, *arXiv:2007.01911*. [Online]. Available: http://arxiv.org/abs/2007.01911

[9] L. Han, G. Cheng, G. Han, R. Ma, and W. Zhang, "Electronically beam-steering antenna with active frequency-selective surface," *IEEE Antennas Wireless Propag. Lett.*, vol. 18, no. 1, pp. 108–112, Jan. 2019.

[10] A. A. Artemenko, V. N. Ssorin, R. O. Maslennikov, and A. V. Mozharovskiy, "Lens antenna with electronic beam steering capabilities," U.S. Patent 14 593 552, Apr. 30, 2015.

[11] A. A. Artemenko and R. O. Maslennikov, "Electronically beam-steerable antenna device," U.S. Patent 9 590 300, Mar. 7, 2017.

[12] Y. Aslan, J. Puskely, J. H. J. Janssen, M. Geurts, A. Roederer, and A. Yarovoy, "Thermal-aware synthesis of 5G base station antenna arrays: An overview and a sparsity-based approach," *IEEE Access*, vol. 6, pp. 58868–58882, 2018.

[13] A. S. M. Abdellatif, "High performance integrated beam-steering techniques for millimeter-wave systems," Univ. Waterloo, Waterloo, ON, USA, 2015.

[14] T. Lou, X.-X. Yang, H. Qiu, Z. Yin, and S. Gao, "Compact dual-polarized continuous transverse stub array with 2-D beam scanning," *IEEE Trans. Antennas Propag.*, vol. 67, no. 5, pp. 3000–3010, May 2019.

[15] *ThinKom VICTS Technology*. Accessed: Jan. 31, 2021. [Online]. Available: https://www.thinkom.com/technology/

[16] E. B. Lima, S. A. Matos, J. R. Costa, C. A. Fernandes, and N. J. G. Fonseca, "Circular polarization wide-angle beam steering at Ka-band by in-plane translation of a plate lens antenna," *IEEE Trans. Antennas Propag.*, vol. 63, no. 12, pp. 5443–5455, Dec. 2015.

[17] S. A. Matos, E. B. Lima, J. S. Silva, J. R. Costa, C. A. Fernandes, N. J. Fonseca, and J. R. Mosig, "High gain dual-band beam-steering transmit array for SatCom terminals at Ka-band," *IEEE Trans. Antennas Propag.*, vol. 65, no. 7, pp. 3528–3539, Jul. 2017.

[18] S. A. Matos, J. R. Costa, E. Lima, C. A. Fernandes, and N. J. G. Fonseca, "Prototype of a compact mechanically steered Ka-band antenna for satellite on-the-move," in *Proc. IEEE Int. Symp. Antennas Propag. (APSURSI)*, Jun. 2016, pp. 1487–1488.

[19] Y. Wang, J. Ness, A. Abbosh, and R. L. Gilmore, "A directional flat-panel antenna," International Patent WO 2019 157 567 A1, Feb. 15, 2019.

[20] M. U. Afzal and K. P. Esselle, "Steering the beam of medium-to-high gain antennas using near-field phase transformation," *IEEE Trans. Antennas. Propag.*, vol. 65, no. 4, pp. 1680–1690, Apr. 2017.

[21] M. U. Afzal and K. P. Esselle, "High-gain beam steering by near-field phase transformation—An overview," in *Proc. IEEE Int. Symp. Antennas Propag. USNC/URSI Nat. Radio Sci. Meeting*, Jul. 2018, pp. 1447–1448.

[22] M. U. Afzal and K. P. Esselle, "A low-profile, planar, power-efficient 2D beam-steering antenna technology," in *Proc. Int. Conf. Electromagn. Adv. Appl. (ICEAA)*, Sep. 2018, pp. 232–235.
[23] K. Singh, M. U. Afzal, M. Kovaleva, and K. P. Esselle, "Controlling the most significant grating lobes in two-dimensional beam-steering systems with phase-gradient metasurfaces," *IEEE Trans. Antennas Propag.*, vol. 68, no. 3, pp. 1389–1401, Mar. 2020.
[24] K. K. Katare, A. Biswas, and M. J. Akhtar, "Near-field phase modulation using a semicircular radially gradient metasurface for beam steering of an RF antenna," *J. Comput. Electron.*, vol. 18, no. 2, pp. 671–679, Jan. 2019.
[25] Z. Zhang, H. Luyen, J. H. Booske, and N. Behdad, "X-band, mechanically-beam-steerable lens antenna exploiting the Risley prism concept," *IET Microw., Antennas Propag.*, vol. 14, no. 14, pp. 1902–1908, Nov. 2020.
[26] K. K. Katare, A. Biswas, and M. J. Akhtar, "Microwave beam steering of planar antennas by hybrid phase gradient metasurface structure under spherical wave illumination," *J. Appl. Phys.*, vol. 122, no. 23, Dec. 2017, Art. no. 234901.
[27] X. Zhao, C. Yuan, L. Liu, S. Peng, Q. Zhang, L. Yu, and Y. Sun, "All-metal beam steering lens antenna for high power microwave applications," *IEEE Trans. Antennas Propag.*, vol. 65, no. 12, pp. 7340–7344, Dec. 2017.
[28] Q. Tang, B. H. Mcguyer, E. Booen, S. Saraswat, F. Tabatabai, H. Bolandhemmat, C. Von Badinski, and W. H. Theunissen, "Flat-panel mechanical beam steerable array antennas with in-plane rotations: Theory, design and low-cost implementation," *IEEE Open J. Antennas Propag.*, vol. 2, pp. 679–688, 2021.
[29] X. Zhao, C. Yuan, L. Liu, S. Peng, Q. Zhang, and H. Zhou, "All-metal transmit-array for circular polarization design using rotated cross-slot elements for high-power microwave applications," *IEEE Trans. Antennas Propag.*, vol. 65, no. 6, pp. 3253–3256, Jun. 2017.
[30] J. Wang and Y. Ramhat-Samii, "Phase method: A more precise beam steering model for phase-delay metasurface based Risley antenna," in *Proc. URSI Int. Symp. Electromagn. Theory (EMTS)*, May 2019, pp. 1–4.
[31] A. A. Baba, R. M. Hashmi, K. P. Esselle, M. Attygalle, and D. Borg, "A millimeter-wave antenna system for wideband 2-D beam steering," *IEEE Trans. Antennas Propag.*, vol. 68, no. 5, pp. 3453–3464, May 2020.
[32] M. Chen, E. Abdo-Sánchez, A. Epstein, and G. Eleftheriades, "Theory, design, and experimental verification of a reflectionless bianisotropic Huygens' metasurface for wide-angle refraction," *Phys. Rev. B, Condens. Matter*, vol. 97, no. 12, 2018, Art. no. 125433.
[33] G. Lavigne, K. Achouri, V. S. Asadchy, S. A. Tretyakov, and C. Caloz, "Susceptibility derivation and experimental demonstration of refracting metasurfaces without spurious diffraction," *IEEE Trans. Antennas Propag.*, vol. 66, no. 3, pp. 1321–1330, Mar. 2018.
[34] G. Lavigne, K. Achouri, V. Asadchy, S. Tretyakov, and C. Caloz, "Refracting metasurfaces without spurious diffraction," 2017, *arXiv:1705.09286*. [Online]. Available: http://arxiv.org/abs/1705.09286
[35] H.-P. Li, G.-M. Wang, T. Cai, J.-G. Liang, and X.-J. Gao, "Phase- and amplitude-control metasurfaces for antenna main-lobe and sidelobe manipulations," *IEEE Trans. Antennas Propag.*, vol. 66, no. 10, pp. 5121–5129, Oct. 2018.

KHUSHBOO SINGH (Member, IEEE) received the B.Tech. degree, with near-perfect GPA, in electronics and communication engineering from SHIATS, India, in 2012, the M.S. degree by research degree in electronics and communication engineering from LNMIIT, India, in 2014, and the Ph.D. degree in electronics engineering from Macquarie University, Sydney, Australia, in 2021.

From 2014 to 2015, she was an Assistant Professor with the Pratap Institute of Technology and Science, India. From 2015 to 2016, she was a Guest Lecturer with Swami Rama Himalayan University, India. She is currently a Research Associate with the University of Technology Sydney and an Honorary Postdoctoral Associate with Macquarie University. She is also working on the development and optimization of satellite-terminal antenna technology for LEO and MEO. Her research interests include antennas, phase-gradient metasurfaces, beam-steering antennas, frequency selective surfaces, evolutionary optimization methods, artificial intelligence, and machine learning in electromagnetics, surface electromagnetics, waveguide polarizers, and couplers.

Dr. Khushboo has received several awards and scholarships during her academic and professional career. She was awarded a silver medal and certificate of merit on completion of her undergraduate degree. She received a prestigious merit-based LNMIIT scholarship during her master studies with a complete fee waiver and a stipend of INR 15 000 per month, from 2012 to 2014. She was a recipient of the highly competitive Australian government-funded iRTP scholarship for her Ph.D. She received the Choose Maths grant from the Australian Mathematical Sciences Institute (AMSI) to present her work at the AMSI optimize conference in New Zealand, in 2017. During her Ph.D., she received a five-month paid internship with a total grant of $ 26*K* under the Australian Postgraduate Research Intern (APR) Program funded by the National Research Internships Program in collaboration with AMSI. She was also a part of the team that received $ 24*K* from research collaboration under Australia-Germany Joint Research Cooperation Scheme.

MUHAMMAD U. AFZAL (Senior Member, IEEE) received the bachelor's degree (Hons.) in electronics engineering and the master's degree in computational science and engineering from the National University of Sciences and Technology (NUST), Islamabad, in 2009 and 2011, respectively, and the Ph.D. degree in electronics engineering from Macquarie University, Australia, in 2017.

He started his professional career as a Laboratory Engineer with the Research Institute for Microwave and Millimetre-Wave Studies (RIMMS), NUST, in 2010. He was promoted to a Lecturer, in 2012, which he continued till February 2013. After his Ph.D., he was offered a postdoctoral position for a period of three years on a project funded by the Australian Research Council (ARC) through the Discovery Grant Scheme at Macquarie University, in 2017. Apart from the project-specific research, he has co-supervised one Ph.D., three master's of research, and several undergraduate thesis students at Macquarie University. He is currently a Research Fellow with the University of Technology Sydney. He developed the concept of near-field phase transformation during his Ph.D. research, which was demonstrated to enhance the directivity of low-gain aperture antennas in the IEEE TAP paper entitled "Dielectric Phase-Correcting Structures for Electromagnetic Band-Gap Resonator Antennas." He is the co-inventor of efficient antenna beam-steering technology referred to as near-field meta-steering. This technology received the "Highly Commended" certificate in the Five Future-Shaping Research Priorities category in the 2017 Academic Staff Awards at Macquarie University. To commercialize the outcomes of his research, he led a team of colleagues in a CSIRO-sponsored ON Prime 2 in 2017, a pre-accelerator program designed to commercialize outcomes of academic research in Australia. He is also working on the development of satellite-terminal antenna technology. His research interests include electromagnetic phase-shifting structures, frequency selective surfaces, and similar metamaterials for microwave and millimeter-wave antenna applications.

Dr. Afzal has received several awards and scholarships, including a merit-based scholarship in six out of eight semesters during the undergraduate degree, a scholarship of complete fee waiver during the postgraduate degree, and the international Macquarie Research Excellence (iMQRES) scholarship towards doctorate study from Macquarie University. He received a Competitive Travel Grant in 2015 to present his research work at a flagship conference under the Antennas and Propagation Society (APS) in Vancouver, Canada. He assisted in preparing several grant applications, including a successful ARC Discovery Grant in 2018. He was the third CI in a team of five who received a grant of more than $ 20*K* from the German Academic Exchange Service in a funding scheme "Australia-Germany Joint Research Co-Operation Scheme."

KARU P. ESSELLE (Fellow, IEEE) received the B.Sc. degree (Hons.) in electronic and telecommunication engineering from the University of Moratuwa, Sri Lanka, and the M.A.Sc. and Ph.D. degrees with near-perfect GPA in electrical engineering from the University of Ottawa, Canada.

He was the Director of the WiMed Research Centre and an Associate Dean-Higher Degree Research (HDR) of the Division of Information and Communication Sciences and directed the Centre for Collaboration in Electromagnetic and Antenna Engineering, Macquarie University. He is currently the Distinguished Professor of electromagnetic and antenna engineering with the University of Technology Sydney and a Visiting Professor with Macquarie University, Sydney. According to 2019 Special Report on Research published by The Australian National Newspaper, he is the National Research Field Leader in Australia in both microelectronics and electromagnetisms fields. He has authored over 600 research publications and his articles have been cited over 11 000 times. His publications received over 1200 citations, in 2020. His H-index is 52 and i-10 is 191. He is in world's top 100 000 most-cited scientists list by Mendeley Data. Since 2002, his research team has been involved with research grants, contracts, and Ph.D. scholarships worth about 20 million dollars, including 15 Australian Research Council grants, without counting the 245 million-dollar SmartSat Corporative Research Centre, which started, in 2019. His research has been supported by many national and international organizations, including Australian Research Council, Intel, U.S. Air Force, Cisco Systems, Hewlett-Packard, Australian Department of Defence, Australian Department of Industry, and German and Indian governments. He has provided expert assistance to more than a dozen companies, including Intel, Hewlett Packard Laboratory (USA), Cisco Systems (USA), Audacy (USA), Cochlear, Optus, ResMed and Katherine-Werke (Germany). His team designed the high-gain antenna system for the world's first entirely Ka-band CubeSat made by Audacy, USA and launched to space by SpaceX, in December 2018. This is believed to be the first Australian-designed high-gain antenna system launched to space, since CSIRO-designed antennas in Australia's own FedSat launched, in 2002. He is in the College of Expert Reviewers of the European Science Foundation (2019–2022) and he has been invited to serve as an international expert/research grant assessor by several other research funding bodies as well, including the European Research Council and funding agencies in Norway, Belgium, The Netherlands, Canada, Finland, Hong Kong, Georgia, South Africa, and Chile. He has been invited by the Vice-Chancellors of Australian and overseas universities to assess applications for promotion to professorial levels. He has also been invited to assess grant applications submitted to Australia's most prestigious schemes, such as Australian Federation Fellowships and Australian Laureate Fellowships. In addition to the large number of invited conference speeches he has given, he has been an invited plenary/extended/keynote speaker of several IEEE and other conferences and workshops, including EuCAP 2020 Copenhagen, Denmark; URSI'19 Seville, Spain; and 23rd ICECOM 2019, Dubrovnik, Croatia.

Dr. Esselle has also served as a member for the Dean's Advisory Council and the Division Executive and as the Head of the Department several times. He is a fellow of the Royal Society of New South Wales and Engineers Australia. His awards include Runner-Up to 2020 Australian National Eureka Prize for Outstanding Mentor of Young Researchers, the 2019 Motohisa Kanda Award (from IEEE USA) for the Most Cited Paper in IEEE TRANSACTIONS ON ELECTROMAGNETIC COMPATIBILITY in the past five years, the 2019 Macquarie University Research Excellence Award for Innovative Technologies, the 2019 ARC Discovery International Award, the 2017 Excellence in Research Award from the Faculty of Science and Engineering, the 2017 Engineering Excellence Award for Best Innovation, the 2017 Highly Commended Research Excellence Award from Macquarie University, the 2017 Certificate of Recognition from IEEE Region 10, the 2016 and 2012 Engineering Excellence Awards for Best Published Paper from IESL NSW Chapter, the 2011 Outstanding Branch Counselor Award from IEEE Headquarters (USA), the 2009 Vice Chancellor's Award for Excellence in Higher Degree Research Supervision, and the 2004 Innovation Award for Best Invention Disclosure. His mentees have been awarded many fellowships, awards, and prizes for their research achievements. Fifty-five international experts who examined the theses of his PhD graduates ranked them in the top 5% or 10%. Two of his recent students were awarded Ph.D. with the highest honor at Macquarie University–the Vice Chancellor's Commendation. From 2018 to 2020, he chaired the prestigious Distinguished Lecturer Program Committee of the IEEE Antennas and Propagation (AP) Society the premier global learned society dedicated for antennas and propagation which has close to 10 000 members worldwide. After two stages in the selection process, he was also selected by this Society as one of two candidates in the ballot for 2019 President of the Society. Only three people from Asia or Pacific apparently have received this honor in the 68-year history of this Society. He is also one of the three Distinguished Lecturers (DL) selected by the Society in 2016. He is the only Australian to Chair the AP DL Program ever, the only Australian AP DL in almost two decades, and second Australian AP DL ever (after UTS Distinguished Visiting Professor Trevor Bird). From 2015 to 2020, he has served the IEEE AP Society Administrative Committee in several elected or ex-officio positions. He is also the Chair of the Board of Management of Australian Antenna Measurement Facility, and was the elected Chair of both IEEE New South Wales (NSW), and IEEE NSW AP/MTT Chapter, in 2016 and 2017. He is a Track Chair of IEEE AP-S 2021 Singapore and AP-S 2020 Montreal, a Technical Program Committee Co-Chair of ISAP 2015, APMC 2011, and TENCON 2013, and the Publicity Chair of ICEAA/IEEE APWC 2016, IWAT 2014, and APMC 2000. He has served as an Associate Editor for IEEE TRANSACTIONS ON ANTENNAS PROPAGATION, *IEEE Antennas and Propagation Magazine*, and IEEE ACCESS.